NeuroImage 71 (2013) 147–157

Contents lists available at SciVerse ScienceDirect

NeuroImage

journal homepage: www.elsevier.com/locate/ynimg

Temporal prediction errors modulate cingulate–insular coupling

Roberto Limongi [a,b,*], Steven C. Sutherland [a], Jian Zhu [a], Michael E. Young [c], Reza Habib [a]

[a] Southern Illinois University Carbondale, USA
[b] Venezuelan Institute for Scientific Research, Venezuela
[c] Kansas State University, USA

ARTICLE INFO

Article history:
Accepted 29 December 2012
Available online 17 January 2013

Keywords:
Dynamic causal models
Prediction error
Cingulate cortex
Insular cortex
Predictive behavior

ABSTRACT

Prediction error (i.e., the difference between the expected and the actual event's outcome) mediates adaptive behavior. Activity in the anterior mid-cingulate cortex (aMCC) and in the anterior insula (aINS) is associated with the commission of prediction errors under uncertainty. We propose a dynamic causal model of effective connectivity (i.e., neuronal coupling) between the aMCC, the aINS, and the striatum in which the task context drives activity in the aINS and the temporal prediction errors modulate extrinsic cingulate–insular connections. With functional magnetic resonance imaging, we scanned 15 participants when they performed a temporal prediction task. They observed visual animations and predicted when a stationary ball began moving after being contacted by another moving ball. To induced uncertainty-driven prediction errors, we introduced spatial gaps and temporal delays between the balls. Classical and Bayesian fMRI analyses provided evidence to support that the aMCC–aINS system along with the striatum not only responds when humans predict whether a dynamic event occurs but also *when* it occurs. Our results reveal that the insula is the entry port of a three-region pathway involved in the processing of temporal predictions. Moreover, prediction errors rather than attentional demands, task difficulty, or task duration exert an influence in the aMCC–aINS system. Prediction errors debilitate the effect of the aMCC on the aINS. Finally, our computational model provides a way forward to characterize the physiological parallel of temporal prediction errors elicited in dynamic tasks.

Introduction

The neural coding of predictive behavior has gained substantial attention in the last decade (Bar, 2009). Research on predictive behavior includes areas as diverse as neuroeconomics (Platt and Huettel, 2008), learning (Behrens et al., 2007; den Ouden et al., 2009; O'Doherty et al., 2001; O'Doherty et al., 2004), and brain function (Friston and Kiebel, 2009). In all these domains, researchers test their theories using both animal and human models.

Human predictive behavior comprises the prediction of the outcome of an event: the winner of a football match, whether it will rain, or which product will sell better. Critically, humans also predict the temporal dynamics of events. For example, while walking down the street, a person might witness a rear-end collision. As an anticipatory physiological response, the witness' body may shrink away a few milliseconds before the collision. The witness not only predicts the occurrence of the collision but also *when* the collision occurs.

Prediction error likelihood is associated with a linear increase in the activity of the anterior mid-cingulate cortex (aMCC, Brown and Braver, 2005).[1] Furthermore, in tasks demanding either time processing (Kosillo and Smith, 2010), the prediction of an event's onset (Forster and Brown, 2011), or predictions under uncertainty (Singer et al., 2009) activity in the anterior insula (aINS) increases. For the current study, we consider crucial, however, that uncertainty in the outcomes of future events conjointly increases the activity of the aMCC and the aINS (Critchley et al., 2001).

The aMCC and the aINS constitute an input–output system (Medford and Critchley, 2010; Taylor et al., 2009) with anatomical (Mesulam and Mufson, 1982; Mufson and Mesulam, 1982) and functional (Taylor et al., 2009) reciprocal connectivity. These facts suggest that effective connectivity (i.e., neuronal coupling) might mediate the functional aMCC–aINS connectivity in uncertainty-related temporal prediction tasks. Based upon the observed BOLD responses elicited during a temporal prediction task that generated different levels of uncertainty in the participants, we used a dynamic causal modeling (DCM) approach (Friston et al., 2003) to test two hypotheses. First, task context (i.e., the main effect of temporal prediction) would directly increase within-region coupling in the aINS. Second, signals

* Corresponding author at: 8424 NW 56th St., Suite CCS 00202, Doral, FL 33166, USA. Fax: +58 212 5041764.
E-mail address: Roberto.Limongi@fulbrightmail.org (R. Limongi).

1053-8119/$ – see front matter © 2013 Elsevier Inc. All rights reserved.
http://dx.doi.org/10.1016/j.neuroimage.2012.12.078

[1] According to the four-region neurobiological model of the cingulate organization (Vogt, 2009; Vogt et al., 2003), the aMCC comprises the caudal parts of areas 32, 24, and 33 encompassed between the vertical plane of the anterior commissure and the diagonal from the vertical plane of the genu of the corpus callosum.

associated with prediction errors would modulate the connection strength of the aMCC–aINS system.

From a DCM perspective, regional activity in the aMCC–aINS system can be produced via either direct or modulatory inputs. The main effect of an uncertainty-related prediction task is an increment of the insula's hemodynamic response (Critchley et al., 2001). Thus, we predicted that a model generating the fMRI data would include direct inputs to the aINS. In addition, neural activity associated with prediction errors modulates cortical–cortical (den Ouden et al., 2009) and cortical–subcortical (den Ouden et al., 2010) connections. Therefore, we predicted that temporal prediction errors would modulate aMCC–aINS connections. No previous studies, however, allowed us to anticipate whether prediction errors would modulate forward or backward connections. Thus, we evaluated this issue via model comparison.

Because the BOLD response is unspecific for excitatory and inhibitory connections that instantiate cortical activity (Logothetis, 2012). Our study relied on two assumptions regarding the dynamics of the synaptic plasticity within and between our regions of interest. First, synaptic plasticity of cortical within-region intrinsic connections comprises changes in both excitatory and inhibitory neuronal subpopulations. Second, between-region extrinsic inter-regional connections comprise changes mainly in excitatory couplings (Douglas and Martin, 2004). Thus, we assumed that direct influence of task context would produce changes in both excitatory and inhibitory connections whereas temporal prediction errors would cause changes only in aMCC–aINS extrinsic connections.

We tested our predictions in two stages. First, we identified a set of inter-regional connections in an optimal DCM. Several candidate models with different interregional configurations could accommodate our hypotheses and assumptions. By means of model comparison, we selected the model with the highest probability of having produced the fMRI data. To represent a more realistic decision making circuit in the model, we also added connections from the ventral striatum. Second, we tested our optimal model against models with alternative direct and modulatory inputs.

Temporal prediction task

We used a variant of a task that has been traditionally used in research on causation: the Michotte's launching effect task (Thines et al., 1990). Participants predicted the movement's onset of a stationary ball contingent to the contact of a second ball. In this basic condition, the movement's onset of the stationary ball was highly predictable because the spatiotemporal contiguity between both balls cued the launching time (see Supplemental Video 1). We introduced different levels of uncertainty by modifying this basic stimulus in the temporal and spatial dimensions. In the temporal dimension, we introduced two delays between the termination of the first ball's movement and the onset of the stationary ball's movement. Empirical data and mathematical models support the thesis that subjective time is not linearly related to objective time (Beckmann and Young, 2009; Catania, 1970; Gibbon, 1977, 1981; Gibbon and Church, 1981; Young et al., 2005). Failing to predict an objective sensory magnitude produces uncertainty in future predictions (Schultz et al., 2008; Singer et al., 2009), which increases the probability of committing prediction errors. Although in our task the trial instructions informed the participants on the duration of the programmed delay, higher uncertainty for longer delays was expected. In some timing tasks, individual differences in prediction accuracy arise due to variations in the strategy that participants might adopt for time estimation. For example, when participants are instructed to predict long durations spontaneous language-based counting increases the accuracy. The use of this chronometric strategy could confound the interpretation of the fMRI data (Hinton et al., 2004). In our task, however, chronometric timing unlikely caused any individual differences because the delays lasted less than 1500 ms. In the spatial dimension, we introduced two different spatial discontiguities (gaps). The effect of delay depends on the spatial gap between the objects (Young et al., 2005). Thus, for example, for a given delay we expected greater uncertainty-driven prediction errors in the presence of large gaps than in the presence of small gaps.

In this task, the computational value of each prediction error could produce adjustments in subsequent predictions. More accurate adjustments, however, would occur after explicitly delivering objective feedback (e.g., "your prediction was 230 ms late") as an instance of supervised learning. Nevertheless, because we wished to ensure a high level of error commission across trials for the same condition (to avoid ceiling effects) we did not deliver feedback after the familiarization trials.

Modeling prediction errors

In previous fMRI studies using prediction errors as either a covariate (e.g., in linear models of the hemodynamic responses) or as exogenous inputs (e.g., in dynamic causal models), the experimenters have not used a direct measure of such errors. They have created continuous distributions of either the prediction errors or the probabilities of committing such errors. To construct the distributions, they have estimated the most-likely parameter values of theoretical behavioral models. Examples of these types of models are the Rescorla–Wagner model (Rescorla and Wagner, 1972), the temporal difference model (Sutton and Barto, 1998), and the Bayesian learning models (Behrens et al., 2007; den Ouden et al., 2010; Mathys et al., 2011). In the Rescorla–Wagner and the temporal difference models, the investigators estimate the free parameters (e.g., the learning rate) and then use such estimators to compute the prediction errors (O'Doherty et al., 2007). Conversely, by means of Bayesian learning the investigators construct distributions of prediction-error probabilities.

Although these strategies account for the behavioral data and serve the purpose of constructing continuous distributions that enter fMRI/DCM models, they implicitly rely on the assumption that the models mirror how the brain executes the tasks. Consequently, the problem of selecting the best possible behavioral model accompanies these strategies (see, for example, den Ouden et al., 2010). Because there always exists a more probable behavioral model that could produce a prediction-error/probabilities distribution, the investigator remains uncertain of the exact relationship between the neurophysiological and the behavioral data. To avoid this problem, we used a model-free direct measure of temporal prediction errors as a continuous variable.

Materials and methods

Participants

Fifteen right handed students (10 female), between 19 and 26 years of age (M = 21.76, SD = 2.26) and with no neurological history participated in the study. Participants signed informed consent forms and received a $25 gift card for participating. The study was approved by the Human Subjects Committee of Southern Illinois University at Carbondale.

Stimuli

The stimulus set consisted of nine types of visual animations with three gap sizes (0, 1, and 2 cm; 0.0, 0.9, and 1.9° of visual angle respectively) and three delay durations (0, 300, and 1200 ms). Each animation lasted 2700 ms and began with two balls appearing on the computer screen, one ball to the left of the screen and the other ball in the middle of the screen. Each ball was 1.34 cm (1.28° of visual angle) in diameter. At the beginning of each animation sequence, the left-most ball began to move to the right and continued at a constant

speed until it stopped at the programmed gap. The second ball would begin moving to the right at the programmed delay (Fig. 1, and see Supplemental Video 2 for an example of the conditions—long delay and large gap).

Paradigm

Fig. 1 illustrates the progression of a single trial. A 2000 ms written verbal cue indicated the type of event to predict (e.g., no gap and short delay). The cue was followed by a fixation point for 540 ms and the programmed animation for 2700 ms. Thus, every trial lasted 5240 ms. Trial duration was not a multiple of the scanner repetition time (2500 ms) in order to ensure an effective sampling of the hemodynamic response (Henson, 2007). At the beginning of each session, instructions directed the participant to press the right index finger when he or she believed the second ball would begin moving. During the week before the scanning day, the participants performed familiarization trials with feedback (e.g., "your prediction was 235 ms faster"). They performed additional familiarization trials on the scanning day. After the in-scanner practice trials, the participants executed 693 trials divided into eleven sessions (with the exception of one participant who executed 630 trials divided into 10 sessions). Trial type, as determined by combinations of spatial gaps and temporal delays, was randomized within each session, and no feedback on performance was given during the fMRI scans.

Behavioral data analysis

We analyzed the absolute value of the prediction errors. We decided to use the absolute values based upon behavioral and physiological criteria (see Subsection "Bayesian model comparison of posterior probability maps" for the physiological justification). At a behavioral level, absolute values better index the response profiles across conditions. That is, absolute values directly assess prediction error variability regardless of the error direction (Young et al., 2005). With a standard analysis of variance of absolute prediction errors (launching time − response time), Young and collaborators found that the underlying distributions of the experimental conditions differed with respect to the mean; longer delays produced greater prediction errors across gaps. Thus, we chose a linear model as a preliminary analysis of the behavioral data. This linear model succeeded at replicating Young et al.'s findings. However, because we aimed at obtaining a clear picture of how the experimental conditions affected the entire distribution of prediction errors, we conducted an ex-Gaussian distributional analysis.

The aggregated distribution of temporal prediction errors approximates the shape of a reaction-time distribution (i.e., right skewed) observed in two-choice decision tasks (Ratcliff and McKoon, 2008). The literature reports different model-fitting strategies to model reaction times. Differences especially arise when the investigator aims at modeling not only the response time but also the response accuracy. In addition, different assumptions on the cognitive mechanisms that produce the responses orient the selection of the theoretical distribution. However, when the response time is the main variable of interest, the ex-Gaussian distribution seems appropriate for two reasons. First, it allows an intuitive interpretation of the experimental effects on the shape of the distribution (Matzke and Wagenmakers, 2009). Second, its parameters allow to execute means comparisons like those used in conventional frequentist tests (e.g., *t*-test).

The ex-Gaussian distribution convolves a Gaussian distribution and an exponential distribution. Three parameters describe the distribution. Mu (μ) and sigma (σ) capture the Gaussian's moments whereas tau (τ) captures the effect of the exponential function (Lacouture and Cousineau, 2008). Differences in μ yielded by experimental conditions drive a shift in the distribution. Differences in σ reflect changes in its breadth (i.e., dispersion). And differences in τ reflect changes in the

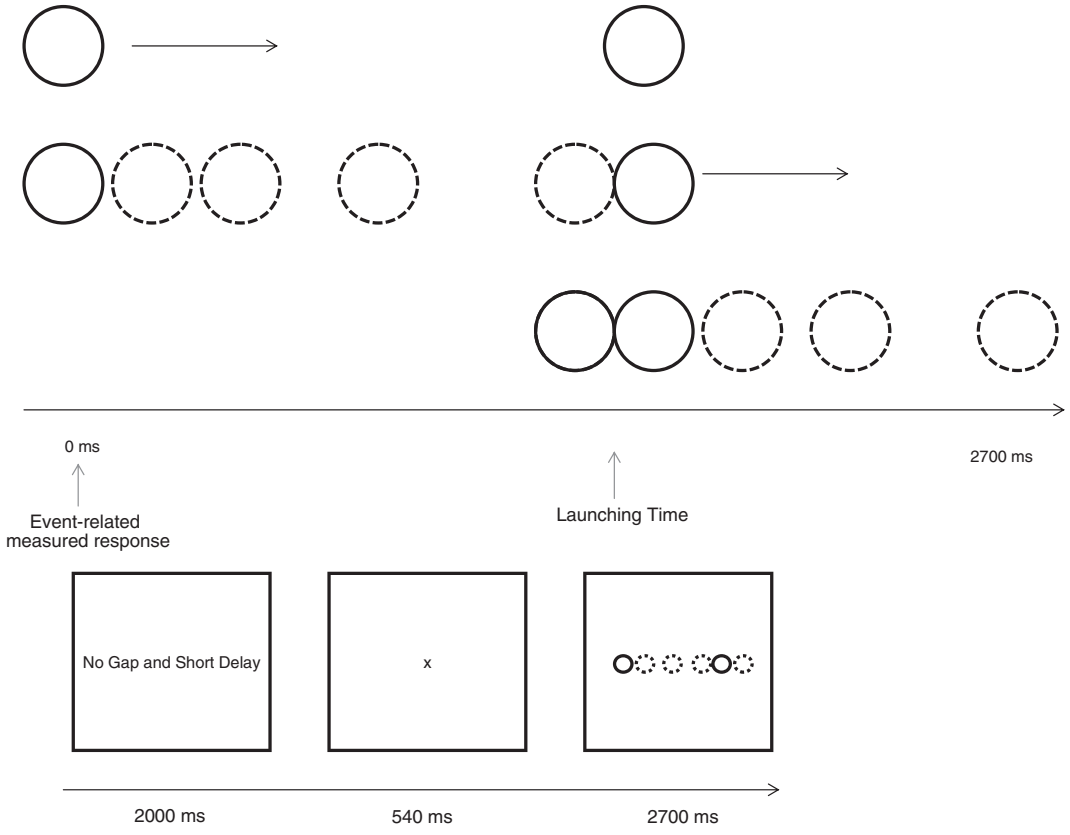

Fig. 1. Stimulus and task. Animation sample of a collision of two balls (top) and timeline of a single trial (bottom).

tail of the distribution. The algebraic sum of μ and τ approximates the mean of the distribution. We fit the ex-Gaussian model to the prediction errors condition-wise per subject. The resulting parameters were independently subjected to a standard repeated measures analysis of variance. Finally, we collapsed the prediction errors across gaps and delays and computed the mean absolute values of prediction errors in 10% Vincentiles. This latter procedure allowed us to visualize the relation between the magnitude of the BOLD response elicited at the stimulus onsets and the magnitude of the prediction error computed at the launching times.

Functional magnetic resonance imaging

Image acquisition

Images were acquired with an ascending interleaved slice acquisition protocol in a Philips Intera 1.5-T magnet using a standard head coil. Each experimental session (11 for 14 participants and 10 for one participant) comprised the acquisition of 141 contiguous whole brain volumes (T2* single-shot echo-planar image, time repetition = 2500 ms, time echo = 50 ms, flip angle = 90°, field of view = 220 × 220 mm^2, 64 3 64 matrix, 3.44 × 3.44 × 5.5 mm voxels, 26 × 5.5-mm axial slices, 0-mm gap). The first 8 images were discarded to allow for T2 equilibrium effect, and the remaining 133 volumes were taken to functional analysis. Upon completion of the functional acquisition, high-resolution T1 weighted 3D structural images were acquired.

Preprocessing

Images were assessed for quality assurance before preprocessing, and all of the fMRI analysis steps were performed in SPM8 (Wellcome Trust Centre for Neuroimaging, London, UK; http://www.fil.ion.ucl.ac.uk/spm). Functional images were time corrected to the middle slice and realigned. A Gaussian smoothing kernel with the full-width at half maximum (FWHM) set to 5 mm was applied to the images before estimating the realignment parameters, and image registration was applied to the first volume. All images were resliced, and a mean image was created from the whole resulting set. The anatomical image was coregistered to this image followed by gray-matter segmentation. Rigid alignment was applied to the segmented tissue with a 1.5 × 1.5 × 1.5 voxel size resolution. Non-linear deformation was subsequently performed for final realignment, the creation of the group anatomical template, and the creation of the participants' flow fields. The template was later normalized to the MNI space and spatially smoothed with preserved concentration and 8 mm FWHM of Gaussian convolution. Individual's flow fields and the group's anatomical template were used to transform the functional images to the MNI space with 3 × 3 × 3 mm voxel size. The normalized functional images were finally smoothed with an 8 mm FWHM of Gaussian convolution and no-modulation.

FMRI models and data analysis

Bayesian model comparison of posterior probability maps (PPMs). The distributional analysis of the absolute prediction errors fulfilled our behavioral data analysis objectives. However, we still sought evidence that the absolute prediction errors better accounted for changes in the BOLD responses across conditions than the raw prediction errors or than delayed and early errors separately (as suggested by one of our reviewers). To decide among these three possibilities, we performed a Bayesian model selection (BMS) with subjects as random effects (Rosa et al., 2010).

We fit each subject's functional data to four linear models in an event-related manner locked at the stimulus onsets. All four models included task context as an event of interest. Delay (rescaled to the 0–1 range), and gap (rescaled to the 0–1 range) were included as parametric modulators. Upon this basic set of regressors, we constructed the four models with additional parametric modulators. The first model (M1) included only the absolute values of prediction errors. The second model (M2) included separate regressors for delayed and early errors. The third model (M3) included a regressor with absolute errors and a regressor with binomial values (1 and 0). These values represented early and delayed responses respectively. The fourth model (M4) included a column vector for raw errors. Each parametric regressor was convolved with the canonical hemodynamic response function and orthogonalized between each other (confirmed via the orthogonality matrix in SPM8). We also included the 6-head movements' parameters as additional regressors of no interest to exclude the proportion of non-experiment-driven variance from the error term. A high-pass filter (128 s) was applied to each time course to filter out low frequency noise. Serial correlations in the time series were accounted for via autoregressive modeling. To fulfill our main objectives, a mask image comprising the aMCC and the aINS was created. However, the literature consistently reports that an essential circuit of temporal decision making also involves the ventral striatum and the ventromedial prefrontal cortex (Delgado and Tricomi, 2011; O'Doherty, 2011). Therefore for a comprehensive description of our temporal prediction neural circuit, masks with these regions were also included. The non-smoothed normalized images were use in the estimation of the log-evidence maps per model and per subject. Finally, we smoothed the maps with an 8 mm FWHM of Gaussian convolution.

To address the question of which model would have the highest probability of producing the obtained BOLD responses across subjects, we conducted a Bayesian estimation of the PPMs (γ) and of the exceedance probability maps (EPM, φ, the probability that a given model be more likely to produce the BOLD response at a specific voxel than any other model). Subjects were included as random effects. We thresholded the PPMs at γ = 0.75 and the EPMs at φ = 0.95 (Rosa et al., 2010). The model with the highest EPM was selected.

Classical first and second level analyses of statistical parametric maps (SPMs) and second level Bayesian analysis. After selecting the winning model as described above, we reestimated the parameters of this model by means of the restricted maximum likelihood method (i.e., classical SPM first-level analysis) voxel-wise across the participant's segmented gray matter of the whole brain volume. We then entered the participants' contrast images of the effects of interest (task, delay, gap, and prediction error) into a random-effects group analysis. We performed two types of whole-brain analysis. We first identified statistically significant positive and negative hemodynamic responses by means of a standard one-sided *t*-test with a conservative cluster-wise control of family-wise error rate with $p < .05$ corrected at a cluster level (each cluster of minimum size of two voxels). Although this threshold effectively protected us against committing Type I error, it could have prevented us from detecting otherwise significant activity in non-surviving voxels. Thus, we also performed a Bayesian second level analysis of the parameter estimates to identify voxels with probability of being active higher than 95%.

Bilinear dynamic causal models

By means of bilinear differential equations, we estimated the model parameters that captured changes in the intrinsic (i.e., within-region) coupling between inhibitory and excitatory neuronal subpopulations and the modulation of extrinsic (i.e., between-region) coupling of excitatory neuronal subpopulations (i.e., extrinsic connections). We also evaluated the neurophysiologically inspired parameter structure of the optimal model to disentangle the sign (increment or decrement) and magnitude (rate of change) of both the direct effect of task context and the modulatory effect of prediction errors. From the observed BOLD responses, we estimated these parameters as the best predictors of the hemodynamics that gave rise to the observed time series. Critically, we

defined and tested our model's structure and parameters' values within the BMS framework and by frequentist tests, respectively.

Model space and parameter structure motivation and definition

To effectively test our hypotheses and assumptions, we first needed to select an optimal model: a model with the most likely set of aMCC–aINS endogenous (i.e., forward, backward, or bidirectional) connections and connections between this system and the striatum. We selected the optimal model from a 36-model space constructed in two steps. First, we constructed an essential model space comprising four possible combinations of aMCC–aINS connections based upon anatomical constraints and our a priori hypotheses (Stephan et al., 2010). In all four models, we added task-context direct inputs to the aINS and prediction-error modulatory inputs to either the backward or forward cingulate–insular connections. These basic constraints constituted the four-model essential space (Fig. 2). Second, we crossed nine possible combinations of endogenous connections (forward, backward, or bidirectional) with the four aMCC–aINS combinations of the essential model space. The partition expanded to 36 models (Fig. 2).

Because we explicitly assumed that changes in within-region connectivities affected both excitatory and inhibitory connections and that changes in inter-regional connectivities affected mainly excitatory connections, we believed that a two-state model would better account for the BOLD responses than a traditional single state model. Two-state models describe changes in excitatory and inhibitory connections separately (Marreiros et al., 2008). Thus, to determine the optimal model we fit all 36 candidate models by means of the two-state algorithm approach. However, we compared the resulting two-state optimal model against a single-state model to test our assumption (see Sections "Optimal model's structure and parameters testing" and "Optimal model test"). At a parameter level, we did not aim to determine the source of the modulatory signals but only the rate of change of the synaptic strength in the extrinsic connections as a function of the prediction errors.

Time series extraction

At the group level, we identified the local maxima of activity elicited by prediction errors in both the aINS and the aMCC. We also identified the local maxima of activity elicited by task context (i.e., main effect of task) in the ventral striatum (putamen). At the participant level, we extracted the times series (first eigenvector) of the participant's maxima detected within an 8-mm sphere of the group maximum yielded by the classical (for the aMCC and the aINS) and Bayesian (for the striatum) second level analyses. We failed to detect above-threshold activity in the aINS in one participant and in the aMCC in another participant. Thus, we used data from only 13 participants.

Optimal model selection

Identifying the optimal model consisted of two comparisons at a family level and one comparison at a model level. Although our optimal model would encompass aMCC–aINS modulatory inputs, we needed to remove the uncertainty of whether those inputs would affect forward or backward connections. To this aim, we partitioned the

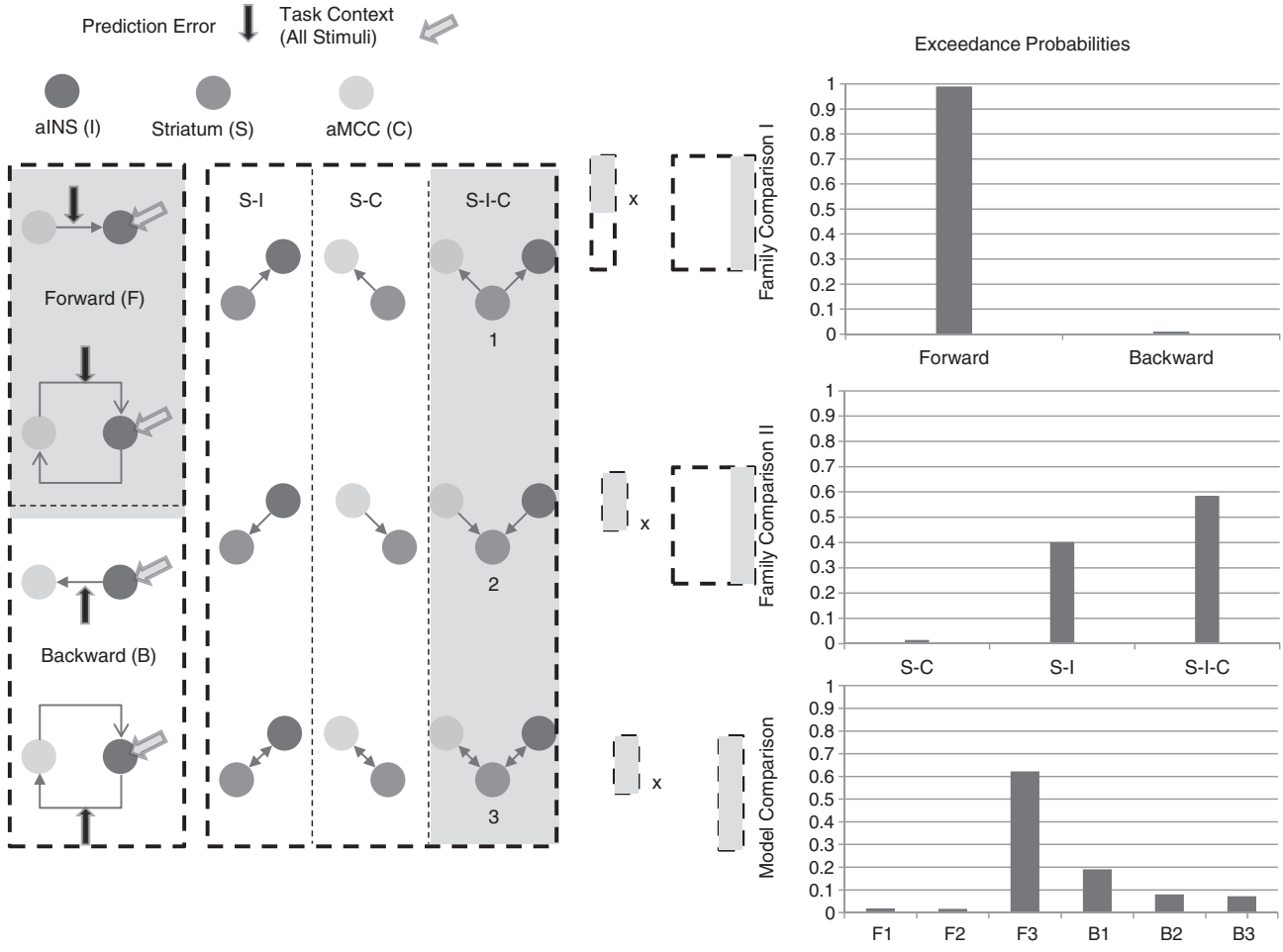

Fig. 2. Model space and Bayesian family/model comparison for the optimal model selection. The essential model space (leftmost dashed rectangle) crosses connections originating in the striatum (right dashed rectangle). Bar graphs show the exceedance probabilities of both family and model comparisons. The optimal model comprised aMCC–aINS forward connections and full bidirectional connections from the striatum.

36-model space into two families (one family of models with forward modulatory and one family of models with backward modulatory aMCC–aINS connections). Both families were subjected to a family model comparison. With the winning family, we then answered the question of whether the striatum would effectively interact with the aMCC–aINS system through connections to a single region (aMCC or aINS) or through connections to both regions. Thus, we partitioned the winning family into three new families defined by the presence of forward, backward, or bidirectional connections originating in the striatum. A new family model comparison was performed. Finally, we selected the optimal model with striatal–cingulate–insular connections by determining the best model from the resulting winning family (Fig. 2).

Inference at family and model levels conformed to BMS procedures with random effects at a group level as a suitable approach to balance goodness of fit, complexity (Forster, 2000; Myung, 2000; Pitt et al., 2002; Zucchini, 2000), and between-subject variability (Penny et al., 2010; Stephan et al., 2009). We used the negative variational free energy of the system as a surrogate of the log-model evidence, and we computed the exceedance probability (φ) by means of Gibbs sampling. Family/model selection followed the identification of the highest φ.

Optimal model's structure and parameter testing

After optimizing our model, we tested our main hypotheses against alternative configurations of direct and modulatory inputs. We created four alternative models, three such following a single-state approach to additionally test for alternative within-region dynamics. In model 1 (A1), task context modulated self-connections in the aINS. In Model 2 (A2), not only prediction error but also task context modulated cingulate–insular connections. Model 3 (A3) mimicked the configuration of the optimal model but followed a single-state algorithm. In Model 4 (A4), task-context modulated aMCC–aINS forward connections and prediction error drove activity in the aINS. Finally, model 5 (A5) included task-context driven activity in the striatum because task context elicited activity in the right putamen (see Bayesian results, Section "Classical and Bayesian second level analysis"). Estimation of A1, A2, and A3 followed a single-stage approach whereas estimation of A4 and A5 followed a two-state approach. To test our optimal model's parameters (i.e., the estimates of the direct effect of task and the modulatory effect of prediction errors), we subjected each parameter estimate to a frequentist *t*-test as an across-subjects random effects analysis.

Results

Behavioral

Trials with absolute prediction errors greater than 1500 ms were excluded (14 of 10,332 trials in total). Fig. 3 shows the results of the ex-Gaussian distributional analysis. Delays caused changes in μ, $F(2, 28) = 5.45$, $p < .001$. Long delays produced large absolute errors and, in consequence, shifted the distribution to the right. However, neither gaps, $F(2, 28) = .10$, $p = .90$, nor the Delay × Gap interaction, $F(4, 56) = .82$, $p = .52$, reached statistical significance. Similarly, delay durations also affected σ, $F(2, 28) = 3.51$, $p = .04$. Long delays produced more error variability. Neither gaps, $F(2, 28) = .15$, $p = .86$, nor the Delay × Gap interaction, $F(4, 56) = .63$, $p = .64$, reached statistical significance. Finally, both the delays, $F(2, 28) = 18.60$, $p < .001$, and their interaction with gap sizes produced changes in τ, $F(2, 28) = 5.96$, $p < .001$. Long delays lengthened the tail of the distribution and large gaps likewise did so but only in the absence of a delay. The main effect of gap did not reach significance, $F(2, 28) = 2.38$, $p = .11$. A conservative post-hoc Tukey's honestly significant difference test revealed that short delays more strongly affected both μ and σ than no delays whereas long delays affected τ more than both short and no delays. That is, no delays and short delays shifted the distribution of prediction errors to the right whereas long delays skewed the distribution to the right. Large gaps increased the skewness of the distribution more than small gaps and no gaps when no delays were present.

The ex-Gaussian distributional analysis offers a clear picture of how the task conditions induced temporal prediction errors in terms of how they affected the shape of the distribution. The mean of an ex-Gaussian distribution approximates the algebraic sum of μ and τ. While μ mainly determined the mean values in the no-delay and short-delay conditions, τ mostly determined the mean value in the long delay condition. Likewise, the ex-Gaussian analysis revealed that τ mostly determined the increase in the mean prediction error across gaps in the no-delay level. Finally, the description by Vincentiles revealed that the prediction errors increased linearly in the lowest Vincentiles and exponentially in the highest Vincentiles (Fig. 4). This fact is important for purposes of relating the effects of the absolute prediction errors with the magnitude of the BOLD responses.

FMRI

Bayesian model comparison

We examined the PPMs of all four models to determine which model showed voxels surviving the threshold of $\gamma = 0.75$. We initially expected that either M2 (the model with separate delayed and early responses) or M3 (the model with absolute values and the additional regressor coding early and delayed responses) would show the highest probability of producing the hemodynamic responses. The results, however, surprised us. We found voxels surviving our predefined threshold only in the model with absolute prediction errors (M1, Fig. 4). In addition, we found voxels surviving our pre-specified threshold in the aINS, the aMCC, and the striatum but not in the ventromedial prefrontal cortex. The exceedance probabilities in the voxels showing the highest posterior probabilities surpassed our predefined threshold of $\varphi = 0.95$. Based on this Bayesian analysis, we justified the use of absolute values of temporal prediction errors as a more accurate predictor of the BOLD responses. Moreover, these results warrant a discussion on the implications regarding the physiological interpretation of the absolute prediction errors (see The physiological parallel of our prediction error measure section).

Classical and Bayesian second level analysis

We examined the SPM results to know which brain areas showed increased activity when the participants prepared to predict the temporal occurrence of the second ball's launch (i.e., main effect of task). As predicted, activity in the left and right aINS was associated with task execution (see Inline Supplementary Table S1 for activations detected in the classical whole brain analysis and Fig. 4 for images).

Inline Supplementary Table S1 can be found online at http://dx.doi.org/10.1016/j.neuroimage.2012.12.078.

We then examined the SPM results to determine which brain areas were recruited as a linear function of prediction errors. Both the aMCC and the aINS areas showed increased activity. That is, the activity of the right aMCC, right aINS, and left aINS increased in linear relation to the absolute prediction error. Fig. 4 shows the percent signal changes in both regions disaggregated by 10 percentiles. Peak activity occurred approximately 5 s after stimulus onset, and activity increased as a function of Vincentiles. We note that the size of the effect increased at the highest Vincentiles. That is, as the prediction error approached the tail of the distribution, the effect in both the aMCC and in the aINS increased more. However, we also note that at the lowest Vincentiles—where prediction errors were the smallest—the activity in the aMCC decreased relative to baseline.

A Bayesian second level analysis provided a more meaningful activation map. Specifically, it allowed us to discover that task context had greater than a 95% probability of having produced activity in

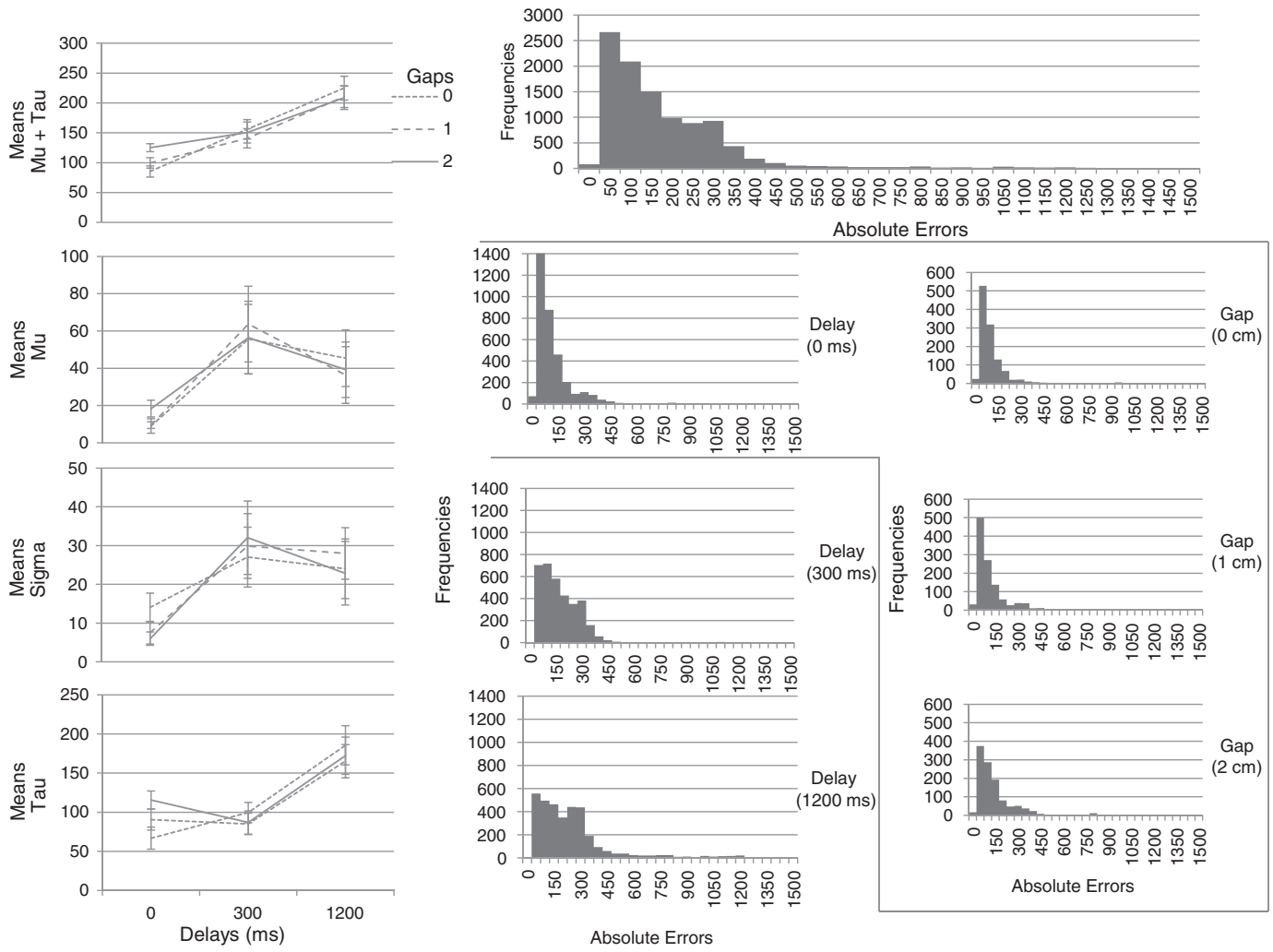

Fig. 3. Distributional analysis of the behavioral data. Distribution of aggregated absolute prediction errors (top right). Distributions of absolute errors collapsed across gaps (middle) and for the three gap levels in the 0 ms delay condition (right). Mean comparisons of ex-Gaussian best parameters (left).

the right putamen but not in the ventromedial prefrontal cortex (see Inline Supplementary Table S2 for a complete list of activations detected in the Bayesian analysis).

Inline Supplementary Table S2 can be found online at http://dx.doi.org/10.1016/j.neuroimage.2012.12.078.

DCM

Optimal model selection and parameter testing

Family comparison revealed that the optimal model belongs to a family of models with forward aMCC–aINS connections as confirmed by an exceedance probability of $\varphi = .99$ compared to a family of models with backward modulatory connections (Fig. 2). Furthermore, the optimal model belongs to a family of models in which both the aMCC and the aINS would connect to the striatum, $\varphi = .59$, when compared to families in which the striatum would connect only to the aMCC or only to the aINS. Six possible models remained for a final model comparison. Models with forward or bidirectional cingulate–insular connections were crossed with forward, backward, and bidirectional striatal–insular and striatal–cingulate connections. A model with bidirectional striatal–insular, bidirectional striatal–cingulate, and forward cingulate–insular connections generated the optimal configuration, $\varphi = .62$.

Optimal model test

Model comparison revealed that our optimal model more likely produced the fMRI data than any of the alternative models ($\varphi = .87$, Fig. 5). Within the aINS, the task context raised the rate of change in neuronal coupling between excitatory and inhibitory neuronal subpopulations; $d = .41$, $SE = .11$, $t_{(12)} = 3.61$, $p = .003$. And, prediction-error-related signals negatively modulated aMCC–aINS excitatory forward connections; $d = -.05$, $SE = .018$, $t_{(12)} = 3.06$, $p = .001$.

Discussion

In this study, we employed a dynamic temporal prediction task in which the participants predicted the movement's onset of a stationary ball. Different levels of uncertainty were manipulated by introducing temporal delays and spatial gaps. Critically, as the delay duration increased across gaps, the predictions were less accurate. Modeling the BOLD responses as parametrically modulated by the prediction errors yielded linear activity in the aMCC and in the aINS. Task context yielded activity in the aINS and in the ventral striatum. Bayesian model comparison showed that a model with only main effect of task and Task × Prediction Errors interaction more likely produced the observed physiological responses. The dynamic causal model revealed two important findings. First, task context involving uncertainty (i.e., the main effect of task) drives insular activity by means of

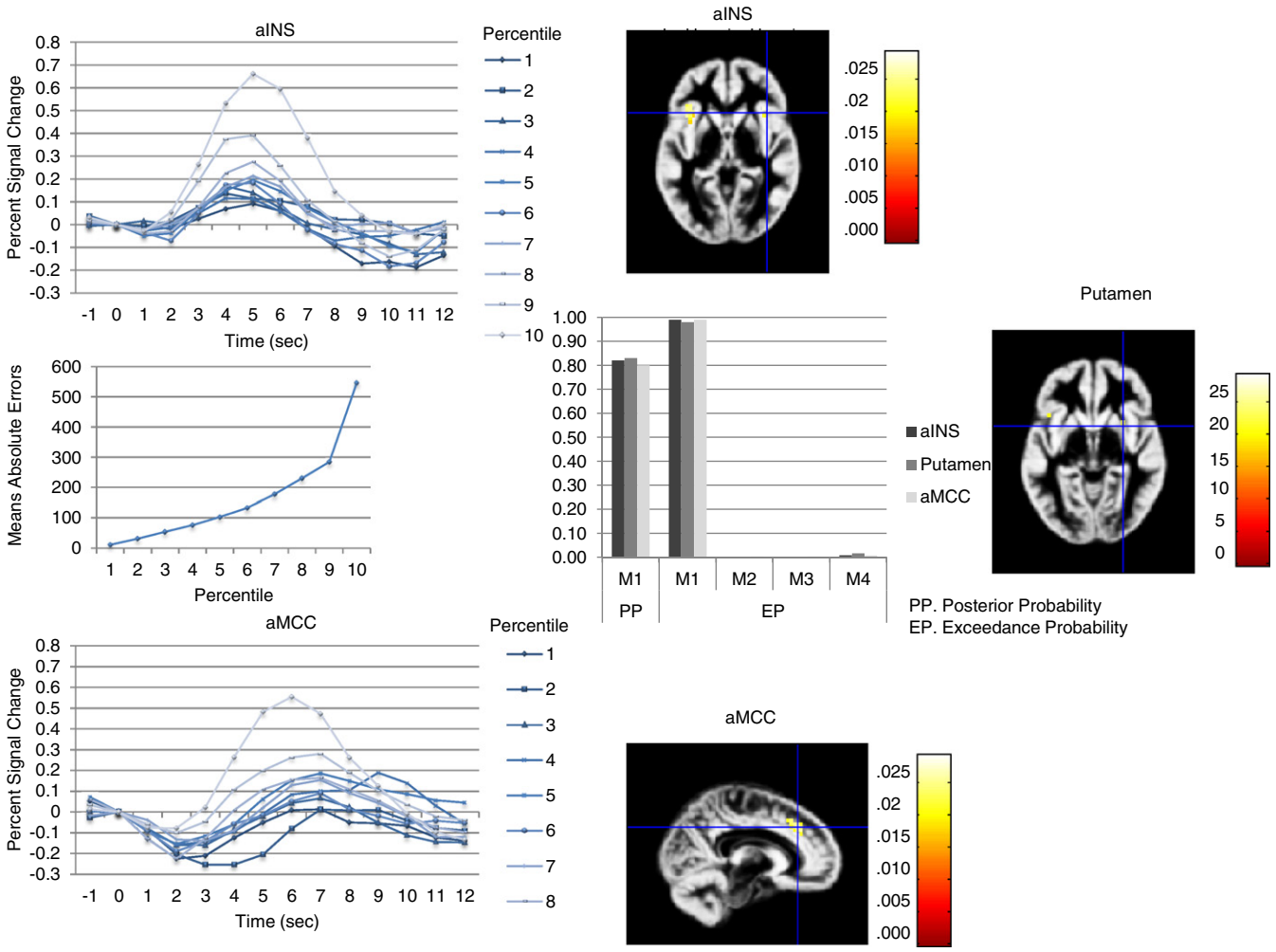

Fig. 4. Activity detected in the right aMCC and right aINS as a function of the absolute prediction errors and activity detected in the right putamen resulting from task-context effect. Overlaid images on the normalized group anatomical template (top and bottom right). Bar graph depicts posterior (PP) and exceedance (EP) probabilities of the four competing GLMs. M1 included only the absolute values of prediction errors. M2 included separate regressors for delayed and early errors. M3 included a regressor with absolute errors and a regressor with binomial values valencing the errors. M4 comprised a column vector for raw errors. Peristimulus time histograms (left) and aggregated absolute prediction errors (center right) of 10% Vincentiles. The histograms were constructed by deconvolving the peristimulus time courses of the different events from each another via finite impulse response modeling (Gläscher, 2009).

direct inputs. Second, error-related afferent signals associated with the event's timing (i.e., Task × Prediction Errors interaction) modulate cingulate–insular connections. Circumscribed in the dynamics of the aINS–aMCC system associated with predictive behavior, these findings inform on the role of the system in predictions under uncertainty and the role of prediction errors in the flow of information from the aMCC to the aINS. They also provide a way forward to characterize the physiological parallel of temporal prediction errors in dynamic tasks.

Prediction errors rather than attentional demands, task difficulty, or task duration are associated with activity in the aMCC–aINS system

We witness a debate in the literature regarding the influence of three potential confounding factors on both prediction errors and time estimation: task difficulty (Kosillo and Smith, 2010; Nieuwenhuis et al., 2007), attentional demands, and time on task (Aarts et al., 2008; Brown and Braver, 2005, 2008; Grinband et al., 2011a,b). For example, when subjects are instructed to report differences in the duration of two auditory stimuli, stronger insular activity is elicited in the difficult condition (when the durations differ between 30 ms and 40 ms) than in the easy condition (when the durations differ between 100 and 130 ms, Tregellas et al., 2006). In the studies of the aMCC function, the discussion on the effect of confounding factors is more vivid: More difficult tasks cause higher error rates. But, they also require more time on task, and more attention (Grinband et al., 2011b).

In search for a common theoretical framework, task difficulty and attentional demands can be conceptualized in terms of uncertainty. First, as a task becomes more difficult, the uncertainty on performance increases (Osman, 2010). Thus, the participant needs to accumulate more information (i.e., to reduce uncertainty) by investing more time to make the same accurate decision (Ratcliff and McKoon, 2008). Here, the most uncertain (difficult) conditions (i.e., long delays across gaps) induced the most inaccurate predictions. Second, attention is the estimation of our uncertainty in predicting sensory inputs (Feldman and Friston, 2010). This is, attentional demands increase in the most uncertain conditions. Therefore, regarding attentional demands or task difficulty as confounded with absolute prediction error would seem appealing because large levels of uncertainty produced large prediction errors. To covary out the potential influence of task difficulty and attention, we orthogonalized prediction errors and uncertainty levels (gaps and delays). Prediction errors rather than uncertainty produced aMCC–aINS activity. Third, our task did not include task duration as a confounding factor because time itself constituted the dependent variable.

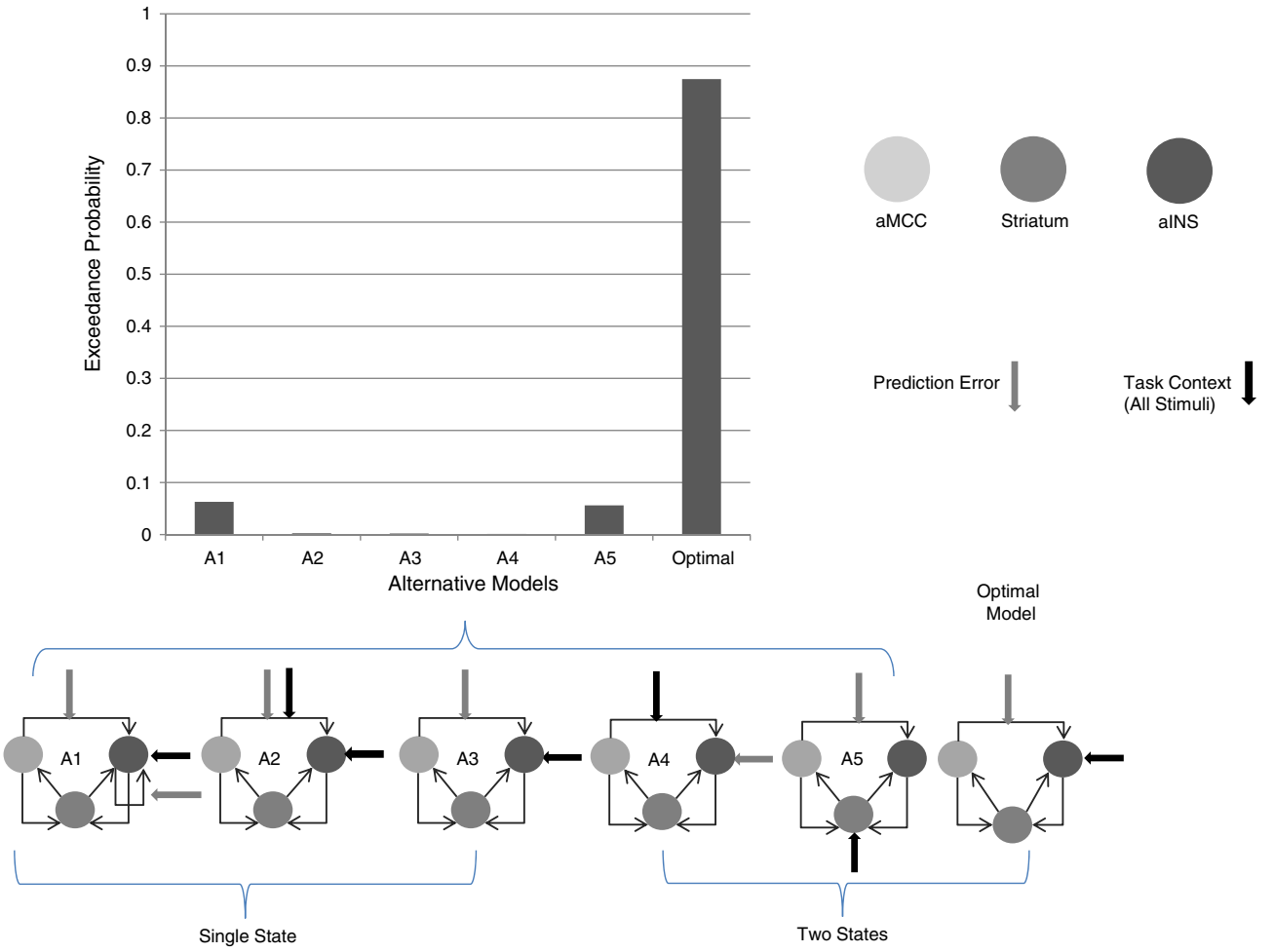

Fig. 5. Exceedance probabilities of 4 alternative and the optimal DCM models.

Prediction errors debilitate the effects of the aMCC on the aINS in a three-region pathway involved in the processing of temporal predictions

Our knowledge on the role of the aMCC in the encoding of prediction errors expands. Previous studies have centered the focus of attention on whether prediction errors activate the aMCC (Alexander and Brown, 2010, 2011; Brown, 2011; Brown and Braver, 2007, 2008; Nee et al., 2011), which have led to the thesis that aMCC is an outcome-predictor region where prediction errors exert an influence (Alexander and Brown, 2011). But, the specific influence had not been identified. Our results elaborate this thesis. Task context directly induces activity in the anterior insula. The insula then exerts an effect on the putamen but not on the aMCC; it is affected by this region. Larger prediction errors debilitate the effects of the aMCC on the aINS by modulating the flow of information from the aMCC to the aINS. But, what is the information that flows from the aMCC to the aINS? And, what is the computational effect of prediction errors over this flow of information?

Critchley (2005) proposed that the aMCC generates anticipated representations of motor responses (efference copies) or predictions and propagates such predictions to the aINS. However, Huettel et al. (2005) suggested that although predictions under uncertainty recruit anterior insular activity the recruitment of the aMCC is conditioned to a task involving learning. Learning involves an update of the predictions and, consequently, the resolution of uncertainty. In theory, the magnitude of the update and uncertainty decreased in subsequent trials. Our fMRI results contradict Huettel and collaborators' hypothesis because the task did not involve learning explicitly but still increased the activity in the aMCC. Thus, Critchley's proposal seems tenable in the context of our results.

In a nonlearning task, it is possible that the modulatory role of prediction error be the same as in learning tasks: to update the prediction that the aMCC maps onto the aINS. Unlike learning tasks, however, the magnitude of the updating process might be constant across consecutive trials. This possibility is worth investigating in tasks where learning is explicitly manipulated; the magnitude of the updating process should decay across trials. Only two other DCM studies have reported the modulatory properties of prediction errors (den Ouden et al., 2009; den Ouden et al., 2010) in learning conditions. However, these studies have not indicated whether prediction errors modulated projections from the aMCC to the aINS.

The physiological parallel of our prediction error measure

The forgoing point draws the discussion to a final important implication of our results: their relation with the heavily documented thesis that the neuronal code associated with the prediction of an event's outcome adapts via dopaminergic signals (Behrens et al., 2007; Contreras-Vidal and Schultz, 1999; O'Doherty et al., 2003; O'Doherty et al., 2007; Schultz, 1994; Schultz, 2010; Schultz et al., 1997; Schultz et al., 2008; Suri, 2002; Suri and Schultz, 1998, 1999, 2001). Phasic suppression of mesencephalic dopaminergic signals elicited after error commission would mediate the learning of the aMCC anticipatory response (Brown and Braver, 2005). Dopaminergic signals would also encode risk prediction, uncertainty (Schultz et al., 2008), long-term reward prediction, and reward prediction error

(Enomoto et al., 2011). Recently, however, Klein-Flügge et al. (2011) provided evidence that signals associated with temporal prediction errors of non-dynamic events originate in the ventral striatum. Indeed, whereas dopaminergic signals exiting the ventral tegmental area might modulate learning in prediction tasks, non-dopaminergic ventral–striatal signals might mirror temporal prediction errors in non-learning tasks. However, these studies focused on how prediction errors modulate the neural code associated with the predictions of non-dynamic stimuli. Therefore, whereas our results expand the domain of the properties of the prediction-error-related modulatory signals from static to dynamic stimuli, they also give rise to a new question: What is the physiological parallel of our prediction error measure? The Bayesian analysis we report here reveals an initial clue to this question as a way forward to future studies.

In the temporal distance approach, prediction errors have been broadly related to dopaminergic activity. Apparently, neural signals associated with temporal prediction error produced in our task do not parallel the phenomenology of prediction errors in the temporal distance approach. This should not come as a surprise for two reasons. First, our task did not include reward delivery as a controlling stimulus in a supervised learning process. Second, more relevant is the fact that dopaminergic signals have positive and negative values (Niv and Schoenbaum, 2008) of prediction errors as one distinctive characteristic, and it is assumed that such errors parallel positive (phasic) and negative (below-tonic) activity of dopaminergic neurons (Aggarwal et al., 2012). Our Bayesian analysis removed such assumption and showed that the absolute prediction error better predicted the physiological responses than the early (positive) and delayed (negative) responses. This finding supports the initial hypothesis that non-dopaminergic signals might relate to temporal prediction errors in non-rewarding dynamic tasks because positive but not negative prediction errors relate to temporal prediction error (Klein-Flügge et al., 2011). This hypothesis is worth investigating. Finally, our study also opens the question of whether the current temporal prediction task with explicit delivery of feedback (i.e., explicit supervised learning) elicits prediction error signals originating in dopaminergic nuclei.

Conclusion

We live in a world with enormous complexity. Thus, we continuously face the challenge of predicting the timing of the events' outcomes. We use temporal predictions at a microscale to make predictions at a macroscale. Imagine that the score of a football game is *tied* just a few seconds before the end of the match, and a penalty kick is awarded to our favorite team. The player taking the penalty kicks, we anticipate the ball's trajectory, and we also anticipate that the goalkeeper will not reach the ball. We certainly predict *when* the ball will cross the goal line. Our body reacts a few milliseconds before the ball crosses the goal line because we predict that our team will win the football game.

The aMCC–aINS system is involved in the processing of dynamic stimuli with temporal uncertainty. Temporal prediction errors modulate the mapping of information between both regions. Temporal prediction of dynamic events' outcomes is, in consequence, an adaptive behavior. This fact suggests a domain-general involvement of this system in the predictive behavior and response selection associated with complex phenomena. We hope that our simple scaled-down paradigm and our statistical approach open new research possibilities to investigate the predictive behavior of complex events.

Supplementary data to this article can be found online at http://dx.doi.org/10.1016/j.neuroimage.2012.12.078.

References

Aarts, E., Roelofs, A., Van Turennout, M., 2008. Anticipatory activity in anterior cingulate cortex can be independent of conflict and error likelihood. J. Neurosci. 28, 4671–4678.

Aggarwal, M., Hyland, B.I., Wickens, J.R., 2012. Neural control of dopamine neurotransmission: implications for reinforcement learning. Eur. J. Neurosci. 35, 1115–1123.

Alexander, W.H., Brown, J.W., 2010. Computational models of performance monitoring and cognitive control. Top. Cogn. Sci. 2, 658–677.

Alexander, W.H., Brown, J.W., 2011. Medial prefrontal cortex as an action–outcome predictor. Nat. Neurosci. 14, 1338–1344.

Bar, M., 2009. Predictions: a universal principle in the operation of the human brain. Philos. Trans. R. Soc. Lond. B Biol. Sci. 364, 1181–1182.

Beckmann, J.S., Young, M.E., 2009. Stimulus dynamics and temporal discrimination: implications for pacemakers. J. Exp. Psychol. Anim. Behav. Process. 35, 525–537.

Behrens, T.E.J., Woolrich, M.W., Walton, M.E., Rushworth, M.F.S., 2007. Learning the value of information in an uncertain world. Nat. Neurosci. 10, 1214–1221.

Brown, J.W., 2011. Medial prefrontal cortex activity correlates with time-on-task: what does this tell us about theories of cognitive control? NeuroImage 57, 314–315.

Brown, J.W., Braver, T.S., 2005. Learned predictions of error likelihood in the anterior cingulate cortex. Science 307, 1118–1121.

Brown, J.W., Braver, T.S., 2007. Risk prediction and aversion by anterior cingulate cortex. Cogn. Affect. Behav. Neurosci. 7, 266–277.

Brown, J.W., Braver, T.S., 2008. A computational model of risk, conflict, and individual difference effects in the anterior cingulate cortex. Brain Res. 1202, 99–108.

Catania, A.C., 1970. Reinforcement schedules and psychophysical judgments. In: Schoenfeld, W.N. (Ed.), The Theory of Reinforcement Schedules. Appleton-Century-Crofts, New York.

Contreras-Vidal, J.L., Schultz, W., 1999. A predictive reinforcement model of dopamine neurons for learning approach behavior. J. Comput. Neurosci. 6, 191–214.

Critchley, H.D., 2005. Neural mechanisms of autonomic, affective, and cognitive integration. J. Comp. Neurol. 493, 154–166.

Critchley, H.D., Mathias, C.J., Dolan, R.J., 2001. Neural activity in the human brain relating to uncertainty and arousal during anticipation. Neuron 29, 537–545.

Delgado, M.R., Tricomi, E., 2011. Reward processing and decision making in the human striatum. In: Mandel, D.R., Vartanian, O. (Eds.), Neuroscience of Decision Making. Psychology Press, New York, NW, pp. 145–172.

den Ouden, H.E.M., Friston, K.J., Daw, N.D., McIntosh, A.R., Stephan, K.E., 2009. A dual role for prediction error in associative learning. Cereb. Cortex 19, 1175–1185.

den Ouden, H.E.M., Daunizeau, J., Roiser, J., Friston, K.J., Stephan, K.E., 2010. Striatal prediction error modulates cortical coupling. J. Neurosci. 30, 3210–3219.

Douglas, R.J., Martin, K.A., 2004. Neuronal circuits of the neocortex. Annu. Rev. Neurosci. 27, 419–451.

Enomoto, K., Matsumoto, N., Nakai, S., Satoh, T., Sato, T.K., Ueda, Y., Inokawa, H., Haruno, M., Kimura, M., 2011. Dopamine neurons learn to encode the long-term value of multiple future rewards. Proc. Natl. Acad. Sci. U. S. A. 108, 15462–15467.

Feldman, H., Friston, K., 2010. Attention, uncertainty and free-energy. Front. Hum. Neurosci. 4, 1–23.

Forster, M.R., 2000. Key concepts in model selection: performance and generalizability. J. Math. Psychol. 44, 205–231.

Forster, S.E., Brown, J.W., 2011. Medial prefrontal cortex predicts and evaluates the timing of action outcomes. NeuroImage 55, 253–265.

Friston, K.J., Kiebel, S.J., 2009. Predictive coding under the free-energy principle. Philos. Trans. R. Soc. Lond. B Biol. Sci. 364, 1211–1221.

Friston, K.J., Harrison, L., Penny, W., 2003. Dynamic causal modelling. NeuroImage 19, 1273–1302.

Gibbon, J., 1977. Scalar expectancy theory and Weber's law in animal timing. Psychol. Rev. 84, 277–325.

Gibbon, J., 1981. On the form and location of the psychometric bisection function for time. J. Math. Psychol. 24, 58–87.

Gibbon, J., Church, R.M., 1981. Time left: linear versus logarithmic subjective time. J. Exp. Psychol. Anim. Behav. Process. 7, 87–107.

Gläscher, J., 2009. Visualization of group inference data in functional neuroimaging. Neuroinformatics 7, 73–82.

Grinband, J., Savitskaya, J., Wager, T.D., Teichert, T., Ferrera, V.P., Hirsch, J., 2011a. Conflict, error likelihood, and RT: response to Brown & Yeung et al. NeuroImage 57, 320–322.

Grinband, J., Savitskaya, J., Wager, T.D., Teichert, T., Ferrera, V.P., Hirsch, J., 2011b. The dorsal medial frontal cortex is sensitive to time on task, not response conflict or error likelihood. NeuroImage 57, 303–311.

Henson, R., 2007. Efficient experimental design for fMRI. In: Friston, K., Ashburner, J., Kiebel, S.J., Nichols, K.A., Penny, W. (Eds.), Statistical Parametric Mapping: The analysis of functional brain images. Elsevier, London, pp. 193–231.

Hinton, S.C., Harrington, D.L., Binder, J.R., Durgerian, S., Rao, S.M., 2004. Neural systems supporting timing and chronometric counting: an FMRI study. Cogn. Brain Res. 21, 183–192.

Huettel, S.A., Song, A.W., McCarthy, G., 2005. Decisions under uncertainty: probabilistic context influences activation of prefrontal and parietal cortices. J. Neurosci. 25, 3304–3311.

Klein-Flügge, Miriam C., Hunt, Laurence T., Bach, Dominik R., Dolan, Raymond J., Behrens, Timothy E.J., 2011. Dissociable reward and timing signals in human midbrain and ventral striatum. Neuron 72, 654–664.

Kosillo, P., Smith, A., 2010. The role of the human anterior insular cortex in time processing. Brain Struct. Funct. 214, 623–628.

Lacouture, Y., Cousineau, D., 2008. How to use MATLAB to fit the ex-Gaussian and other probability functions to a distribution of response times. Tutorial. Quant. Meth. Psychol. 4, 35–45.

Logothetis, N.K., 2012. What we can't do with fMRI. In: G., W.B. (Ed.), MRI and Advanced Imaging in Animals and Humans. Society for Neuroscience, Washington, DC, pp. 7–14.

Marreiros, A.C., Kiebel, S.J., Friston, K.J., 2008. Dynamic causal modelling for fMRI: a two-state model. NeuroImage 39, 269–278.

Mathys, C., Daunizeau, J., Friston, K.J., Stephan, K.E., 2011. A Bayesian foundation for individual learning under uncertainty. Front. Hum. Neurosci. 5, 1–20.
Matzke, D., Wagenmakers, E.-J., 2009. Psychological interpretation of the ex-Gaussian and shifted Wald parameters: a diffusion model analysis. Psychon. Bull. Rev. 16, 798–817.
Medford, N., Critchley, H.D., 2010. Conjoint activity of anterior insular and anterior cingulate cortex: awareness and response. Brain Struct. Funct. 214, 535–549.
Mesulam, M.M., Mufson, E.J., 1982. Insula of the old world monkey. III: efferent cortical output and comments on function. J. Comp. Neurol. 212, 38–52.
Mufson, E.J., Mesulam, M.M., 1982. Insula of the old world monkey. II: afferent cortical input and comments on the claustrum. J. Comp. Neurol. 212, 23–37.
Myung, I.J., 2000. The importance of complexity in model selection. J. Math. Psychol. 44, 190–204.
Nee, D.E., Kastner, S., Brown, J.W., 2011. Functional heterogeneity of conflict, error, task-switching, and unexpectedness effects within medial prefrontal cortex. NeuroImage 54, 528–540.
Nieuwenhuis, S., Schweizer, T.S., Mars, R.B., Botvinick, M.M., Hajcak, G., 2007. Error-likelihood prediction in the medial frontal cortex: a critical evaluation. Cereb. Cortex 17, 1570–1581.
Niv, Y., Schoenbaum, G., 2008. Dialogues on prediction errors. Trends Cogn. Sci. 12, 265–272.
O'Doherty, J.P., 2011. Neural mechanisms underlying reward and punishment learning in the human brain: insights from fMRI. In: Mandel, D.R., Vartanian, O. (Eds.), Neuroscience of Decision Making. Psychology Press, New York, NY, pp. 173–198.
O'Doherty, J., Kringelbach, M.L., Rolls, E.T., Hornak, J., Andrews, C., 2001. Abstract reward and punishment representations in the human orbitofrontal cortex. Nat. Neurosci. 4, 95–102.
O'Doherty, J., Dayan, P., Friston, K.J., Critchley, H.D., Dolan, R.J., 2003. Temporal difference models and reward-related learning in the human brain. Neuron 28, 329–337.
O'Doherty, J., Dayan, P., Schultz, J., Deichmann, R., Friston, K., Dolan, R.J., 2004. Dissociable roles of ventral and dorsal striatum in instrumental conditioning. Science 304, 452–454.
O'Doherty, J.P., Hampton, A., Kim, H., 2007. Model-based fMRI and its application to reward learning and decision making. Ann. N. Y. Acad. Sci. 1104, 35–53.
Osman, M., 2010. Controlling uncertainty: a review of human behavior in complex dynamic environments. Psychol. Bull. 136, 65–86.
Penny, W.D., Stephan, K.E., Daunizeau, J., Rosa, M.J., Friston, K.J., Schofield, T.M., Leff, A.P., 2010. Comparing families of dynamic causal models. PLoS Comput. Biol. 6, 1–14.
Pitt, M.A., Myung, I.J., Zhang, S., 2002. Toward a method of selecting among computational models of cognition. Psychol. Rev. 109, 472–491.
Platt, M.L., Huettel, S.A., 2008. Risky business: the neuroeconomics of decision making under uncertainty. Nat. Neurosci. 11, 398–403.
Ratcliff, R., McKoon, G., 2008. The diffusion decision model: theory and data for two-choice decision tasks. Neural Comput. 20, 873–922.
Rescorla, R.A., Wagner, A.R., 1972. A theory of Pavlovian conditioning: variations in the effectiveness of reinforcement and nonreinforcement. In: Black, A.H., Prokasy, W.F. (Eds.), Classical Conditioning II: Current Research and Theory. Appleton-Century-Crofts, New York, pp. 64–99.
Rosa, M.J., Bestmann, S., Harrison, L., Penny, W., 2010. Bayesian model selection maps for group studies. NeuroImage 49, 217–224.
Schultz, W., 1994. Behavior-related activity of primate dopamine neurons. Rev. Neurol. (Paris) 150, 634–639.
Schultz, W., 2010. Dopamine signals for reward value and risk: basic and recent data. Behav. Brain Funct. 6, 1–9.
Schultz, W., Dayan, P., Montague, P.R., 1997. A neural substrate of prediction and reward. Science 275, 1593–1599.
Schultz, W., Preuschoff, K., Camerer, C., Hsu, M., Fiorillo, C.D., Tobler, P.N., Bossaerts, P., 2008. Explicit neural signals reflecting reward uncertainty. Philos. Trans. R. Soc. Lond. B Biol. Sci. 363, 3801–3811.
Singer, T., Critchley, H.D., Preuschoff, K., 2009. A common role of insula in feelings, empathy and uncertainty. Trends Cogn. Sci. 13, 334–340.
Stephan, K.E., Penny, W.D., Daunizeau, J., Moran, R.J., Friston, K.J., 2009. Bayesian model selection for group studies. NeuroImage 46, 1004–1017.
Stephan, K.E., Penny, W.D., Moran, R.J., den Ouden, H.E.M., Daunizeau, J., Friston, K.J., 2010. Ten simple rules for dynamic causal modeling. NeuroImage 49, 3099–3109.
Suri, R.E., 2002. TD models of reward predictive responses in dopamine neurons. Neural Netw. 15, 523–533.
Suri, R.E., Schultz, W., 1998. Learning of sequential movements by neural network model with dopamine-like reinforcement signal. Exp. Brain Res. 121, 350–354.
Suri, R.E., Schultz, W., 1999. A neural network model with dopamine-like reinforcement signal that learns a spatial delayed response task. Neuroscience 91, 871–890.
Suri, R.E., Schultz, W., 2001. Temporal difference model reproduces anticipatory neural activity. Neural Comput. 13, 841–862.
Sutton, R.S., Barto, A.G. (Eds.), 1998. Reinforcement Learning: An Introduction. MIT Press, Cambridge, MA.
Taylor, K.S., Seminowicz, D.A., Davis, K.D., 2009. Two systems of resting state connectivity between the insula and cingulate cortex. Hum. Brain Mapp. 30, 2731–2745.
Thines, G., Costall, A., Butterworth, G., 1990. Michotte's Experimental Phenomenology of Perception. Lawrence Erlbaum Associates, Hillsdale, NJ.
Tregellas, J.R., Davalos, D.B., Rojas, D.C., 2006. Effect of task difficulty on the functional anatomy of temporal processing. NeuroImage 32, 307–315.
Vogt, B.A., 2009. Regions and subregions of the cingulate cortex. In: Vogt, B.A. (Ed.), Cingulate Neurobiology and Disease. Oxford University Press, New York, pp. 3–30.
Vogt, B.A., Berger, G.R., Derbyshire, S.W.G., 2003. Structural and functional dichotomy of human midcingulate cortex. Eur. J. Neurosci. 18, 3134–3144.
Young, M.E., Rogers, E.T., Beckmann, J.S., 2005. Causal impressions: predicting when, not just whether. Mem. Cognit. 33, 320–331.
Zucchini, W., 2000. An introduction to model selection. J. Math. Psychol. 44, 41–61.